machines

MDPI

Article

Research and Analysis of the Characteristics of the Brushless Doubly-Fed Machine with High-Performance Decoupling Control

Chaoying Xia * and Nannan Wang

School of Electrical and Information Engineering, Tianjin University, No. 92 Weijin Road, Tianjin 300072, China
* Correspondence: xiachaoying@tju.edu.cn; Tel.: +86-182-2235-6392

Abstract: The paper presents the state-space (SS) model of the brushless double-fed machine (BDFM) by taking the negative conjugate (NC) transformation of the power machine's correlation variable when the current source of the control machine is supplied in the m-t reference frame. Based on this, the testing method of machine parameters is given, and the SS model described by five parameters is obtained. The derivation process and realization method of the slip-frequency vector feedback linearization control (SFV-FLC) strategy are given. Then, researching the SS equation in the m-t reference frame by the control machine rotor field-oriented, the relationship between the maximum and minimum output torque and the control machine rotor flux amplitude and slip velocity, the machine parameters are given considering power supply constraints. Finally, the validity of the theoretical analysis is verified by simulation and experiment, and the feasibility of the decoupling control method are also demonstrated.

Keywords: brushless double-fed machine (BDFM); slip frequency vector feedback linearization control (SFV-FLC); load performance; decoupling control

check for updates

Citation: Xia, C.; Wang, N. Research and Analysis of the Characteristics of the Brushless Doubly-Fed Machine with High-Performance Decoupling Control. *Machines* **2023**, *11*, 313. https://doi.org/10.3390/machines11020313

Academic Editor: Wanke Yu

Received: 12 January 2023
Revised: 17 February 2023
Accepted: 19 February 2023
Published: 20 February 2023

1. Introduction

As a new type of motor, BDFM [1–7] can realize multiple operation modes such as asynchronous, synchronous, and double-fed. It can be used as a motor in alternating current (AC) speed-regulating transmission systems, and can also be used in power generation systems. It has a frequency converter small capacity, adjustable speed, and power factor. At the same time, brushes and slip rings are eliminated in BDFM, which not only reduces maintenance costs but also improves the reliability of system operation. Based on the above advantages, BDFM has been widely considered by scientific researchers.

However, compared with ordinary asynchronous motors, BDFM has a complex structure and the characteristics of a high order, many variables, and nonlinear [8] strong coupling. Therefore, the modeling is more complicated, and the design of the controller is difficult. Many researchers at home and abroad have been starting from the BDFM [9–13] design in recent years. The impact of machine-related design factors—such as the inner and outer diameter of the stator and rotor, the pole slots combination, the indexing ratio, the rotor structure, and the turn ratio of the outer and the inner rotor—on the machine performance is studied to improve its torque and power density and obtain a more winder speed range.

At the same time, with the increasing complexity of automation systems, the frequency of system failures due to various uncertain factors is also increasing. At present, many researchers conduct research on intelligent fault detection [14] for nonlinear dynamic systems. However, fault detection [15] can effectively avoid losses caused by system faults, and the complexity of controller design is also a decisive factor in determining faults. Therefore, how to design a simple and effective controller is a problem that needs to be considered. Some scholars have studied the BDFM control strategy, in which [16–18] proposed a vector control. BDFM is defined as two independent subsystems, namely the

power motor subsystem and the control motor subsystem. The power motor subsystem ignores the stator resistance and adopts stator magnetic field orientation, while the control motor subsystem adopts rotor flux orientation. This method not only has a complicated derivation process, but the flux linkage and torque have not been decoupled; moreover, the data acquisition in the experiment is difficult, and the fault [19] rate of the system is high. To simplify the control, [20] proposed a mathematical model of BDFM in a unified coordinate system. The rotor current on the power machine side or the control machine side is conjugated via calculation to make sure that both sides rotate in the same direction concerning the rotor. All variables in the model are direct-current (DC) values under the unified reference system when any flux is selected for orientation. Based on this model, [21,22] adopts stator flux-oriented vector control to realize BDFM active power, reactive power, and speed control. The unified coordinate system model is simpler and more convenient than the dual synchronous coordinate system model. However, the vector sum of the power motor and control motor rotor flux is regarded as the hybrid rotor flux in the unified coordinate system model, resulting in the limitations of the stator flux-oriented control system [21–24].

BDFM is distinct from induction motors. Induction motors can accomplish system decoupling by the rotor field orientation. However, the decoupling control of the BDFM cannot be solved solely by rotor field orientation. Currently, [21–24], based on the unified coordinate system model, has been powered by two-terminal voltage sources, which is inconsistent with the current inner loop design in most practical systems. A BDFM state-space model is established in the arbitrary rotating reference frame to solve this problem. The BDFM input–output feedback linearization control [25,26] (IO-FLC) is derived based on the model. Although [25] and [26] solve the modeling and decoupling control problem, the performance of BDFM under the control method has not been deeply analyzed. Therefore, to make up for the deficiency of [25,26], the SFV-FLC method and performance analysis considering supply constraints are studied in the paper. Based on this, the theoretical derivation and experimental study are carried out.

The difference between this paper and [27] are as follows: First, the control algorithm is different (this paper uses SFL-FLC under the control motor rotor flux orientation, while [27] uses direct torque control (DTC) under the stator flux orientation). Second, the idea of performance analysis and the depth of theoretical analysis are different (because the two adopt different control algorithms, the idea of performance analysis of BDFM, the change rules, and conclusions of the load characteristics are different). Finally, the verification methods are different (the experimental platform is built in the paper, and the proposed control method and performance analysis are fully experimentally verified; however, there is no experimental verification in [27]).

However, the data in the experiment is acquired through sensors or measuring devices, and under the influence of the external environment and stress, the perfect working state cannot be guaranteed, resulting in unreliable signals. Therefore, [28] proposes a fault diagnosis and prediction method, which can evaluate the detection data in real-time, thereby further improving the reliability of the control.

The differences between the paper and [29] are as follows: First, the control objects studied in the paper are different (the research object of the paper is BDFM, while the object of [29] is the Cup Rotor Permanent-Magnet Doubly Fed Machine). Second, the control algorithms are different (the SFL-FLC method is studied in the paper, while [29] adopts the maximum torque per ampere (MTPA) Control Methods, and the derivation ideas and derivation process are different). Then, the derivation process and conclusion of the performance analysis are completely different (BDFM is more complicated in the performance analysis, and the constraint of the power motor voltage equation is considered. Contrarily, the permanent magnet flux is a constant in [29], and there is no voltage constraint equation). Finally, the verification method is different (this paper built an experimental platform to fully verify the proposed control method and performance analysis. Contrarily, [29] only simulated and verified the control algorithm and load characteristics).

The differences between this paper and [30] are as follows: First, the BDFM modeling method is different (this paper adopts the mathematical model under the unified coordinate system, while [30] adopts the mathematical model under the dual synchronous reference frame system). Second, the control methods are different (this paper adopts the SFL-FLC method. Contrarily, [30] adopts the vector control method). Finally, the research ideas and research depths of performance analysis are different (due to the two different control methods, so the derivation process of performance analysis and the load performance analyzed is quite different from the paper).

In addition, [30] and [27] have different control methods, modeling methods, and performance analysis methods, and [30] and [29] have different research objects, control methods, performance analysis ideas, and verification ideas. Therefore, the research content of the paper is of great research significance.

The paper is arranged as follows. Section 2 establishes the SS model in the m-t reference frame. Section 3 shows the SS model in the m-t reference frame when the current source of the control machine is supplied. Section 4 derives the slip frequency vector feedback linearization control algorithm (SFV-FLC). Section 5 solves the load capacity of the BDFM considering supply constraints and analyses the influences of rotor resistance, the control machine rotor flux, and speed on the load boundary. Sections 6 and 7 are the simulations and the experimental verification. Section 8 is the summary of the paper.

2. State-Space Equation Description of the BDFM

The BDFM includes the winding type, squirrel-cage type, and reluctance type, among which the winding type and squirrel-cage type have similar working principles and mathematical models. The winding type BDFM is discussed as an example in this paper. The method and the results obtained are also applicable to the squirrel cage type BDFM.

As shown in Figure 1, the BDFM is composed of two cascaded induction motors connected in series. The induction motor connected to the grid is defined as the power motor (PM), and the induction motor connected to the inverter is defined as the control motor (CM); two sets of rotor windings are connected in reverse order. There is no magnetic coupling between the stator windings of the PM and the CM, only the electrical coupling between the rotor windings. Suppose that the pole-pairs of the PM is p_{p}, the power supply frequency is f_{p}, the pole-pairs of the CM is p_{c}, and the power supply frequency is f_{c}, the relationship between the steady speed of BDFM and the frequency of the two machines is obtained:

$$n_r = \frac{60(f_{\mathrm{p}} + f_{\mathrm{c}})}{p_{\mathrm{p}} + p_{\mathrm{c}}} \tag{1}$$

where n represents the rotating speed, f represents the frequency, and P represents the pole pairs. The subscripts p and c represent the PM and the CM. The subscript r represents the rotor.

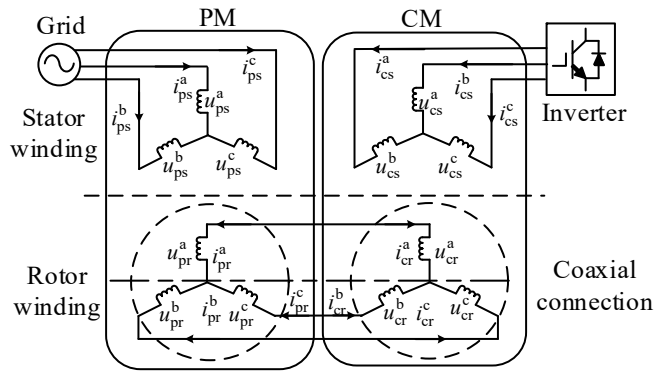

Figure 1. Schematic diagram of BDFM.

The slip frequencies through the rotor windings are as follows:

$$f_s = \frac{p_c f_p + p_p f_c}{p_p + p_c} \tag{2}$$

where the subscript 's' represents the slip.

In (1) and (2), f_p or f_c takes a positive value when the positive phase sequence is supplied, and otherwise takes a negative value. When the control machine is connected to the DC power supply,$f_c = 0$, the speed is called synchronous speed. When $f_c < 0$—the speed is lower than synchronous speed—it is called sub-synchronous operation. When $f_c > 0$—the speed exceeds the synchronous speed—it is referred to as a super-synchronous operation.

Figure 2 depicts the three-phase static reference frame as A-B-C. The two-phase static reference frame is denoted α-β. The three-phase rotor reference frame is a-b-c. the two-phase rotor reference frame is d-q. m-t is the arbitrary rotating reference frame. θ_r is the rotor rotation angle. $\omega_r = d\theta_r/dt$ is the mechanical angular velocity, and m-t is the two-phase arbitrary rotation reference frame. $\lambda = \lambda_c$ is the rotation angle of the m-t reference frame relative to the d-q reference frame.

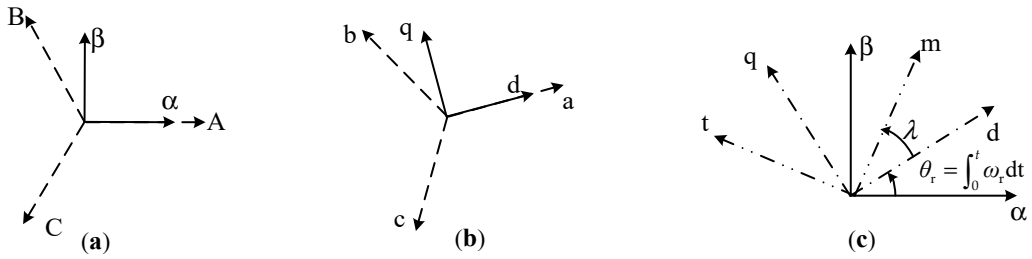

Figure 2. The relationship between the reference frames. (**a**) The relationship between the static stator three-phase reference frame and the static stator two-phase reference frame; (**b**) the relationship between the rotor three-phase reference frame and the rotor d-q reference frame; (**c**) the relationship between the rotor d-q reference frame and the arbitrary rotating m-t reference frame.

The voltage models of the PM in the d-q reference frame are as follows:

$$\begin{aligned} u_{ps}^{dq} &= r_{ps} i_{ps}^{dq} + \mathrm{j} p_p \omega_r (l_{ps} i_{ps}^{dq} + l_{pm} i_{pr}^{dq}) + l_{ps} \dot{i}_{ps}^{dq} + l_{pm} \dot{i}_{pr}^{dq} \\ u_{pr}^{dq} &= r_{pr} i_{pr}^{dq} + l_{pm} \dot{i}_{ps}^{dq} + l_{pr} \dot{i}_{pr}^{dq} \end{aligned} \tag{3}$$

The voltage models of the CM in the d-q reference frame are as follows:

$$\begin{aligned} u_{cs}^{dq} &= r_{cs} i_{cs}^{dq} + \mathrm{j} p_c \omega_r (l_{cs} i_{cs}^{dq} + l_{cm} i_{cr}^{dq}) + l_{cs} \dot{i}_{cs}^{dq} + l_{cm} \dot{i}_{cr}^{dq} \\ u_{cr}^{dq} &= r_{cr} i_{cr}^{dq} + l_{cm} \dot{i}_{cs}^{dq} + l_{cr} \dot{i}_{cr}^{dq} \end{aligned} \tag{4}$$

where the superscript "." represents the derivative of the time, and the subscript p and c represent the PM and the CM, respectively. The subscript s and r represent the stator and rotor, respectively, r, l, l_m represent resistance, inductance, and mutual inductance, respectively, and voltage u, current i, and flux ψ are represented as vectors in the complex form. The superscript dq represents the rotor reference system.

Because the PM and CM rotor windings are coupled in reverse phase order, the rotor voltage and current of the two machines in the d-q reference frame satisfy the following relationship:

$$\begin{aligned} u_{cr}^{dq} &= (u_{pr}^{dq})^* \\ i_{cr}^{dq} &= -(i_{pr}^{dq})^* = \bar{i}_{pr}^{dq} \end{aligned} \tag{5}$$

The superscript "*" and "−" denote conjugate and NC, respectively. Taking the CM rotor current as a reference, defining the rotor current $i_r^{dq} = i_{cr}^{dq} = \bar{i}_{pr}^{dq}$. Taking the NC

operation on both sides of the PM voltage equations in (3), combining the CM's stator and rotor voltage equations in (4), the sixth-order state-space equation of the BDFM in the d-q reference frame is obtained:

$$\dot{x}^{\mathrm{dq}} = A^{\mathrm{dq}}x^{\mathrm{dq}} + B^{\mathrm{dq}}u^{\mathrm{dq}} \tag{6}$$

where, $r_{\mathrm{r}} = r_{\mathrm{cr}} + r_{\mathrm{pr}}$ is the rotor resistance, and $l_{\mathrm{r}} = l_{\mathrm{cr}} + l_{\mathrm{pr}}$ is the rotor inductance.

$$A^{\mathrm{dq}} = \frac{1}{\Delta}\begin{bmatrix} M(-r_{\mathrm{ps}}+\mathrm{j}p_{\mathrm{p}}\omega_{\mathrm{r}}l_{\mathrm{ps}}) & -l_{\mathrm{pm}}l_{\mathrm{cm}}(r_{\mathrm{cs}}+\mathrm{j}p_{\mathrm{c}}\omega_{\mathrm{r}}l_{\mathrm{cs}}) & l_{\mathrm{cs}}l_{\mathrm{pm}}r_{\mathrm{r}}+\mathrm{j}p_{\mathrm{p}}\omega_{\mathrm{r}}Ml_{\mathrm{pm}} - \mathrm{j}p_{\mathrm{c}}\omega_{\mathrm{r}}l_{\mathrm{pm}}l_{\mathrm{cm}}^2 \\ l_{\mathrm{pm}}l_{\mathrm{cm}}(-r_{\mathrm{ps}}+\mathrm{j}p_{\mathrm{p}}\omega_{\mathrm{r}}l_{\mathrm{ps}}) & -N(r_{\mathrm{cs}}+\mathrm{j}p_{\mathrm{c}}\omega_{\mathrm{r}}l_{\mathrm{cs}}) & l_{\mathrm{cm}}l_{\mathrm{ps}}r_{\mathrm{r}}+\mathrm{j}p_{\mathrm{p}}\omega_{\mathrm{r}}l_{\mathrm{cm}}l_{\mathrm{pm}}^2 - \mathrm{j}p_{\mathrm{c}}\omega_{\mathrm{r}}Nl_{\mathrm{cm}} \\ -l_{\mathrm{cs}}l_{\mathrm{pm}}(-r_{\mathrm{ps}}+\mathrm{j}p_{\mathrm{p}}\omega_{\mathrm{r}}l_{\mathrm{ps}}) & l_{\mathrm{cm}}l_{\mathrm{ps}}(r_{\mathrm{cs}}+\mathrm{j}p_{\mathrm{c}}\omega_{\mathrm{r}}l_{\mathrm{cs}}) & -l_{\mathrm{cs}}l_{\mathrm{ps}}r_{\mathrm{r}} - \mathrm{j}p_{\mathrm{p}}\omega_{\mathrm{r}}l_{\mathrm{cs}}l_{\mathrm{pm}}^2+\mathrm{j}p_{\mathrm{c}}\omega_{\mathrm{r}}l_{\mathrm{ps}}l_{\mathrm{cm}}^2 \end{bmatrix}$$

$$B^{\mathrm{dq}} = \frac{1}{\Delta}\begin{bmatrix} M & l_{\mathrm{pm}}l_{\mathrm{cm}} \\ l_{\mathrm{pm}}l_{\mathrm{cm}} & N \\ -l_{\mathrm{cs}}l_{\mathrm{pm}} & -l_{\mathrm{cm}}l_{\mathrm{ps}} \end{bmatrix},\ x^{\mathrm{dq}} = \begin{bmatrix} \dot{\overline{i}}_{\mathrm{ps}}^{\mathrm{dq}} \\ i_{\mathrm{cs}}^{\mathrm{dq}} \\ i_{\mathrm{r}}^{\mathrm{dq}} \end{bmatrix},\ u^{\mathrm{dq}} = \begin{bmatrix} \overline{u}_{\mathrm{ps}}^{\mathrm{dq}} \\ u_{\mathrm{cs}}^{\mathrm{dq}} \end{bmatrix}$$

$$\Delta = l_{\mathrm{ps}}l_{\mathrm{cs}}l_{\mathrm{r}} - l_{\mathrm{cs}}l_{\mathrm{pm}}^2 - l_{\mathrm{ps}}l_{\mathrm{cm}}^2, M = l_{\mathrm{cs}}l_{\mathrm{r}} - l_{\mathrm{cm}}^2, N = l_{\mathrm{ps}}l_{\mathrm{r}} - l_{\mathrm{pm}}^2$$

Each variable in (6) is an AC variable, for which the following rotation transformation is used.

$$x^{\mathrm{mt}} = \mathrm{e}^{-\mathrm{j}\lambda}x^{\mathrm{dq}}$$

The BDFM state-space equation in the m-t reference frame is obtained:

$$\dot{x}^{\mathrm{mt}} = A^{\mathrm{mt}}x^{\mathrm{mt}} + B^{\mathrm{mt}}u^{\mathrm{mt}} \tag{7}$$

where, the superscript mt represents the arbitrary rotating reference frame.

$$A^{\mathrm{mt}} = \frac{1}{\Delta}\begin{bmatrix} M(-r_{\mathrm{ps}}+\mathrm{j}p_{\mathrm{p}}\omega_{\mathrm{r}}l_{\mathrm{ps}}) - \mathrm{j}\Delta\dot{\lambda} & -l_{\mathrm{pm}}l_{\mathrm{cm}}(r_{\mathrm{cs}}+\mathrm{j}p_{\mathrm{c}}\omega_{\mathrm{r}}l_{\mathrm{cs}}) & l_{\mathrm{cs}}l_{\mathrm{pm}}r_{\mathrm{r}}+\mathrm{j}p_{\mathrm{p}}\omega_{\mathrm{r}}\mathrm{M}l_{\mathrm{pm}} - \mathrm{j}p_{\mathrm{c}}\omega_{\mathrm{r}}l_{\mathrm{pm}}l_{\mathrm{cm}}^2 \\ l_{\mathrm{pm}}l_{\mathrm{cm}}(-r_{\mathrm{ps}}+\mathrm{j}p_{\mathrm{p}}\omega_{\mathrm{r}}l_{\mathrm{ps}}) & -N(r_{\mathrm{cs}}+\mathrm{j}p_{\mathrm{c}}\omega_{\mathrm{r}}l_{\mathrm{cs}}) - \mathrm{j}\Delta\dot{\lambda} & l_{\mathrm{cm}}l_{\mathrm{ps}}r_{\mathrm{r}}+\mathrm{j}p_{\mathrm{p}}\omega_{\mathrm{r}}l_{\mathrm{cm}}l_{\mathrm{pm}}^2 - \mathrm{j}p_{\mathrm{c}}\omega_{\mathrm{r}}\mathrm{N}l_{\mathrm{cm}} \\ -l_{\mathrm{cs}}l_{\mathrm{pm}}(-r_{\mathrm{ps}}+\mathrm{j}p_{\mathrm{p}}\omega_{\mathrm{r}}l_{\mathrm{ps}}) & l_{\mathrm{cm}}l_{\mathrm{ps}}(r_{\mathrm{cs}}+\mathrm{j}p_{\mathrm{c}}\omega_{\mathrm{r}}l_{\mathrm{cs}}) & -l_{\mathrm{cs}}l_{\mathrm{ps}}r_{\mathrm{r}}+\mathrm{j}\big(-p_{\mathrm{p}}\omega_{\mathrm{r}}l_{\mathrm{cs}}l_{\mathrm{pm}}^2 + p_{\mathrm{c}}\omega_{\mathrm{r}}l_{\mathrm{ps}}l_{\mathrm{cm}}^2 - \Delta\dot{\lambda}\big) \end{bmatrix}$$

$$B^{\mathrm{mt}} = \frac{1}{\Delta}\begin{bmatrix} M & l_{\mathrm{pm}}l_{\mathrm{cm}} \\ l_{\mathrm{pm}}l_{\mathrm{cm}} & N \\ -l_{\mathrm{cs}}l_{\mathrm{pm}} & -l_{\mathrm{cm}}l_{\mathrm{ps}} \end{bmatrix},\ x^{\mathrm{mt}} = \begin{bmatrix} \dot{\overline{i}}_{\mathrm{ps}}^{\mathrm{mt}} \\ i_{\mathrm{cs}}^{\mathrm{mt}} \\ i_{\mathrm{r}}^{\mathrm{mt}} \end{bmatrix},\ u^{\mathrm{mt}} = \begin{bmatrix} \overline{u}_{\mathrm{ps}}^{\mathrm{mt}} \\ u_{\mathrm{cs}}^{\mathrm{mt}} \end{bmatrix}$$

3. State-Space Equation Description of the Control Machine's Current Source Power Supply

In the control system, flux linkage and torque are usually controlled variables, and the CM is generally designed with a fast-response current loop. The following is the detailed derivation of the BDFM state space description when the current source of the CM is supplied.

The BDFM state-space Equation (8) is obtained, which takes the PM's stator flux, the CM's rotor flux, and the CM's stator current as state variables, and the stator voltage of the PM and the CM as input variables.

$$\begin{bmatrix} \dot{\overline{\psi}}_{\mathrm{ps}}^{\mathrm{mt}} \\ \dot{i}_{\mathrm{cs}}^{\mathrm{mt}} \\ \dot{\psi}_{\mathrm{cr}}^{\mathrm{mt}} \end{bmatrix} = \begin{bmatrix} a_{11} & a_{12} & a_{13} \\ a_{21} & a_{22} & a_{23} \\ a_{31} & a_{32} & a_{33} \end{bmatrix}\begin{bmatrix} \overline{\psi}_{\mathrm{ps}}^{\mathrm{mt}} \\ i_{\mathrm{cs}}^{\mathrm{mt}} \\ \psi_{\mathrm{cr}}^{\mathrm{mt}} \end{bmatrix} + \frac{1}{\Delta}\begin{bmatrix} b_{11} & b_{12} \\ b_{21} & b_{22} \\ b_{31} & b_{32} \end{bmatrix}\begin{bmatrix} \overline{u}_{\mathrm{ps}}^{\mathrm{mt}} \\ u_{\mathrm{cs}}^{\mathrm{mt}} \end{bmatrix} \tag{8}$$

where,
$$a_{11} = -\frac{r_{\mathrm{ps}}}{l_{\mathrm{ps}}}+\mathrm{j}(p_{\mathrm{p}}\omega_{\mathrm{r}} - \dot{\lambda}), a_{22} = -\frac{l_{\mathrm{cm}}^2H+Nl_{\mathrm{ps}}l_{\mathrm{cr}}r_{\mathrm{cs}}}{\Delta l_{\mathrm{ps}}l_{\mathrm{cr}}} - \mathrm{j}p_{\mathrm{c}}\omega_{\mathrm{r}}\frac{N\left(l_{\mathrm{cs}}l_{\mathrm{cr}}-l_{\mathrm{cm}}^2\right)}{\Delta l_{\mathrm{cr}}} - \mathrm{j}\dot{\lambda}$$
$$a_{23} = \frac{l_{\mathrm{cm}}H}{\Delta l_{\mathrm{ps}}l_{\mathrm{cr}}} - \mathrm{j}p_{\mathrm{c}}\omega_{\mathrm{r}}\frac{l_{\mathrm{cm}}N}{\Delta l_{\mathrm{cr}}}, a_{12} = -\frac{l_{\mathrm{pm}}l_{\mathrm{cm}}r_{\mathrm{ps}}}{l_{\mathrm{cr}}l_{\mathrm{ps}}}, a_{13} = \frac{l_{\mathrm{pm}}r_{\mathrm{ps}}}{l_{\mathrm{cr}}l_{\mathrm{ps}}}, a_{21} = -\frac{l_{\mathrm{pm}}l_{\mathrm{cm}}r_{\mathrm{ps}}}{\Delta l_{\mathrm{ps}}}+\mathrm{j}\frac{p_{\mathrm{p}}\omega_{\mathrm{r}}}{\Delta}$$
$$a_{33} = -\frac{H\left(l_{\mathrm{cs}}l_{\mathrm{cr}}-l_{\mathrm{cm}}^2\right)}{\Delta l_{\mathrm{ps}}l_{\mathrm{cr}}} - \mathrm{j}p_{\mathrm{c}}\omega_{\mathrm{r}}\frac{l_{\mathrm{cm}}^2\left(l_{\mathrm{ps}}l_{\mathrm{cr}}-N\right)}{\Delta l_{\mathrm{cr}}} - \mathrm{j}\dot{\lambda}\ , a_{31} = \frac{l_{\mathrm{pm}}\left(l_{\mathrm{cs}}l_{\mathrm{cr}}-l_{\mathrm{cm}}^2\right)}{\Delta l_{\mathrm{ps}}}\left(r_{\mathrm{ps}} - \mathrm{j}p_{\mathrm{p}}\omega_{\mathrm{r}}l_{\mathrm{ps}}\right)$$

$$a_{32} = \frac{l_{cm}H\left(l_{cs}l_{cr}-l_{cm}^2\right)}{\Delta l_{ps}l_{cr}} - jp_c\omega_r\frac{l_{cm}\left(l_{ps}l_{cr}-N\right)\left(l_{cs}l_{cr}-l_{cm}^2\right)}{\Delta l_{cr}} + \frac{l_{cm}r_{cs}\left(l_{ps}l_{cr}-N\right)}{\Delta}, H = l_{pm}^2r_{ps} + l_{ps}^2r_r$$
$$b_{11} = Ml_{ps} - l_{pm}^2l_{cs}, b_{21} = l_{pm}l_{cm}, b_{31} = l_{pm}\left(l_{cm}^2 - l_{cs}l_{cr}\right), b_{12} = 0, b_{22} = N, b_{32} = l_{cm}\left(N - l_{cr}l_{ps}\right)$$

Since $b_{32} \neq 0$, the SS equation of BDFM when the current source of the CM is supplied cannot be obtained simply by removing the CM voltage equation (the second equation) in (8). It is necessary to redefine the CM rotor flux.

Secondly, the stator leakage inductance and rotor leakage inductance cannot be obtained simultaneously by measuring the stator voltage and current. Therefore, it is necessary to convert the PM's stator leakage inductance to the rotor side. According to the principle of constant magnetic field energy storage, it can be obtained that after conversion, r_{ps}, r_{cs}, l_{ps}, and l_{cs} are unchanged, and l_{cm}, l_{pm}, l_{cr}, l_{pr}, σl_{pr}, r_{cr}, r_{pr}, l_r, and Δ have changed. The converted parameter expression is as follows:

$$l'_{cm} = \left(l_{ps}/l_{pm}\right)l_{cm}, l'_{pm} = \left(l_{ps}/l_{pm}\right)l_{pm} = l_{ps}, l'_{cr} = \left(l_{ps}/l_{pm}\right)^2 l_{cr}, l'_r = l'_{cr} + l'_{pr} = \left(l_{ps}/l_{pm}\right)^2 l_r$$
$$\sigma' l'_{pr} = \left(1 - l'^2_{pm}/l'_{ps}l'_{pr}\right)l'_{pr} = \left(1 - l_{pm}^2/l_{ps}l_{pr}\right)\left(l_{ps}^2/l_{pm}^2\right)l_{pr} = l'_{pr} - l_{ps}, l'_{pr} = \left(l_{ps}/l_{pm}\right)^2 l_{pr}$$
$$r'_{cr} = \left(l_{ps}/l_{pm}\right)^2 r_{cr} r'_{pr} = \left(l_{ps}/l_{pm}\right)^2 r_{pr}, r'_r = r'_{cr} + r'_{pr} = \left(l_{ps}/l_{pm}\right)^2 r_r, \Delta' = \left(l_{ps}/l_{pm}\right)^2\Delta$$

where the superscript "," represents the converted parameter.

After conversion, the stator current and flux are invariable. The relation between stator voltage and current is invariable. The rotor current decreases l_{ps}/l_{pm}. The rotor flux increases. The stator and rotor time constant are invariable. Figure 3 includes five machine parameters. The parameters can be obtained by measuring the stator voltage and current.. Single-phase equivalent circuit and BDFM's parameter conversion at stationary is given in Figure 3.

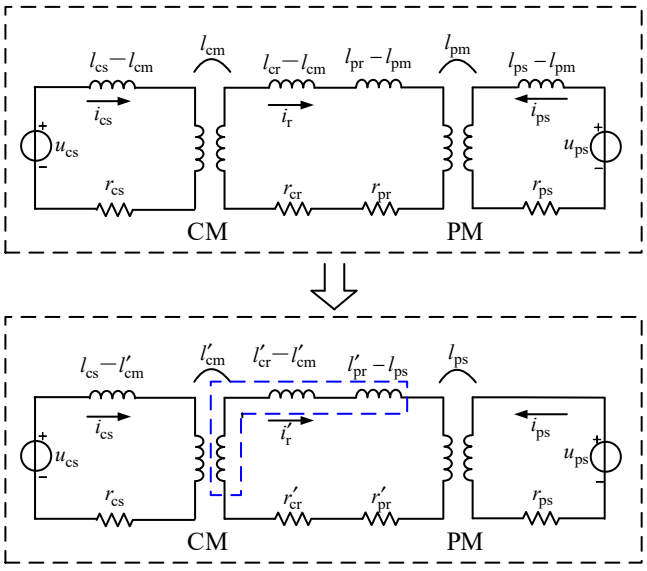

Figure 3. Single-phase equivalent circuit and parameter conversion of BDFM at stationary.

Define a new CM rotor flux linkage as follows:

$$\psi'^{mt}_{cr} = l'_{cm}i^{mt}_{cs} + \left(l'_{cr} + l'_{pr} - l_{ps}\right)i'^{mt}_{r} \tag{9}$$

The newly defined CM rotor inductance includes the PM leakage inductance $l'_{pr} - l_{ps}$ and the CM rotor inductance l'_{cr}. Because $l'_{pr} - l_{ps}$ is much smaller than l'_{cr}, so $\psi'^{mt}_{cr} \approx \psi^{mt}_{cr}$,

the newly defined rotor flux linkage can also reflect the excitation of the CMs magnetic circuit. In [20], the BDFM is a combined model of the flux algebraic equation and the voltage and current differential equation instead of the SS equation model. The rotor flux is defined as the vector sum of the PM and the CM rotor flux linkage. It is easy to see from the equation $r_r i_r^{mt} + j\dot{\lambda}\left(\overline{\psi}_{pr}^{mt} + \psi_{cr}^{mt}\right) = 0$ that when the slip frequency is high for a certain rotor current, maintaining the balance between the rotor-induced voltage and the voltage drop on the rotor resistance, $\overline{\psi}_{pr}^{mt} + \psi_{cr}^{mt}$ will be reduced. The CM and PM rotor flux will appear as two approximately equal sizes, nearly opposite direction vectors. Therefore, the rotor flux amplitude cannot reflect the excitation condition of the rotor magnetic circuit.

Substitute the newly defined rotor flux Equation (9) and the reduced machine parameters into (8). The correlation coefficient is simplified as follows:

$$\frac{N\left(l_{cs}l'_{cr} - l'^2_{cm}\right)}{\Delta' l'_{cr}} = 1,\ \frac{l'_{cm}N}{\Delta' l'_{cr}} = \frac{l_{ps}l'_{cm}}{\Delta'},\ \frac{l'_{pm}\left(l_{cs}l'_{cr} - l'^2_{cm}\right)}{\Delta' l_{ps}} = \frac{1}{l_{ps}},\ \frac{l'_{cm}r'_{cs}\left(l_{ps}l'_{cr} - N\right)}{\Delta'} = 0$$
$$\frac{l'_{cm}H\left(l_{cs}l'_{cr} - l'^2_{cm}\right)}{\Delta' l_{ps}l'_{cr}} = \frac{l'_{cm}\left(r_{ps}+r'_r\right)}{l'_{cr}},\ \frac{l'_{cm}\left(N - l'_{cr}l_{ps}\right)}{\Delta'} = 0,\ \frac{N}{\Delta'} = \frac{l_{ps}l'_{cr}}{\Delta'},\ \frac{l'^2_{cm}l'_{pm} - l'_{pm}l_{cs}l'_{cr}}{\Delta'} = -1$$

Thus, (8) is further simplified as follows:

$$\dot{x}^{mt} = A^{mt}x^{mt} + B^{mt}u^{mt} \tag{10}$$

where,

$$A^{mt} = \begin{bmatrix} -r_{ps}/l_{ps} + j\left(p_p\omega_r - \dot{\lambda}\right) & -l'_{cm}r_{ps}/l'_{cr} & r_{ps}/l'_{cr} \\ -l'_{cm}\left(r_{ps} - jp_p\omega_r l_{ps}\right)/\Delta' & \begin{pmatrix} -l_{ps}l'^2_{cm}\left(r_{ps}+r'_r\right)/\Delta' l'_{cr} \\ -l_{ps}l'^2_{cr}r_{cs}/\Delta' l'_{cr} - j\left(p_c\omega_r + \dot{\lambda}\right) \end{pmatrix} & \begin{pmatrix} l_{ps}l'_{cm}\left(r_{ps}+r'_r\right)/\Delta' l'_{cr} \\ -jp_c\omega_r l_{ps}l'_{cm}/\Delta' \end{pmatrix} \\ \left(r_{ps} - jp_p\omega_r l_{ps}\right)/l_{ps} & l'_{cm}\left(r_{ps}+r'_r\right)/l'_{cr} & -\left(r_{ps}+r'_r\right)/l'_{cr} - j\dot{\lambda} \end{bmatrix}$$
$$B^{mt} = \begin{bmatrix} 1 & 0 \\ l_{ps}l'_{cm}/\Delta' & l_{ps}l'_{cr}/\Delta' \\ -1 & 0 \end{bmatrix}, x^{mt} = \begin{bmatrix} \overline{\psi}_{ps}^{mt} \\ i_{cs}^{mt} \\ \psi'^{mt}_{cr} \end{bmatrix}, u^{mt} = \begin{bmatrix} \overline{u}_{ps}^{mt} \\ u_{cs}^{mt} \end{bmatrix}$$

The SS equation of BDFM is obtained by taking the CM stator current as the input variable:

$$\begin{bmatrix} \dot{\overline{\psi}}_{ps}^{mt} \\ \dot{\psi}'^{mt}_{cr} \end{bmatrix} = \begin{bmatrix} -\frac{r_{ps}}{l_{ps}} + j(p_p\omega_r - \dot{\lambda}) & \frac{r_{ps}}{l'_{cr}} \\ \frac{1}{l_{ps}}(r_{ps} - jp_p\omega_r l_{ps}) & -\frac{r_{ps}+r'_r}{l'_{cr}} - j\dot{\lambda} \end{bmatrix} \begin{bmatrix} \overline{\psi}_{ps}^{mt} \\ \psi'^{mt}_{cr} \end{bmatrix} + \begin{bmatrix} 1 & -\frac{l'_{cm}r_{ps}}{l'_{cr}} \\ -1 & \frac{l'_{cm}(r_{ps}+r'_r)}{l'_{cr}} \end{bmatrix} \begin{bmatrix} \overline{u}_{ps}^{mt} \\ i_{cs}^{mt} \end{bmatrix} \tag{11}$$

The electromagnetic torque equation derived by choosing a newly defined state variable is as follows:

$$T_e = -\frac{p_p}{l'_{cr}} Im\left\{\overline{\psi}_{ps}^{mt}\left(\psi'^{mt}_{cr}\right)^*\right\} + \frac{p_p l'_{cm}}{l'_{cr}} Im\left\{\overline{\psi}_{ps}^{mt}\left(i_{cs}^{mt}\right)^*\right\} + \frac{p_c l'_{cm}}{l'_{cr}} Im\left\{\left(\psi'^{mt}_{cr}\right)^* i_{cs}^{mt}\right\} \tag{12}$$

The equation of motion is,

$$T_e - T_L = J\frac{d\omega_r}{dt} \tag{13}$$

where *Im* represents the imaginary part operation, "*" represents the conjugate transformation, J is the moment of inertia equivalent to the machine shaft, and T_L is the load torque.

4. Description of Control Strategy and Necessary Conditions for Its Implementation

The arbitrary rotating m-t reference frame is oriented along the direction of the CM rotor magnetic field:

$$\psi'^{\ mt}_{cr} = \psi'^{\ m}_{cr} + j\psi'^{\ t}_{cr} = \psi'_{cr} + j0 \tag{14}$$

Substitute (14) into (11), (12) can be written as follows:

$$\dot{\psi}_{cr}^{\prime\ m} = \frac{r_{ps}}{l_{ps}}\overline{\psi}_{ps}^{m} + p_p\omega_r\overline{\psi}_{ps}^{t} - \frac{\left(r_r^{\prime} + r_{ps}\right)}{l_{cr}^{\prime}}\psi_{cr}^{\prime} - \overline{u}_{ps}^{m} + \frac{\left(r_r^{\prime} + r_{ps}\right)l_{cm}^{\prime}}{l_{cr}^{\prime}}i_{cs}^{m} \tag{15}$$

$$0 = \frac{r_{ps}}{l_{ps}}\overline{\psi}_{ps}^{t} - p_p\omega_r\overline{\psi}_{ps}^{m} - \dot{\lambda}\psi_{cr}^{\prime} - \overline{u}_{ps}^{t} + \frac{\left(r_r^{\prime} + r_{ps}\right)l_{cm}^{\prime}}{l_{pm}^{\prime}}i_{cs}^{t} \tag{16}$$

$$T_e = -\frac{p_p}{l_{cr}^{\prime}}\overline{\psi}_{ps}^{t}\psi_{cr}^{\prime} + \left(\frac{p_c l_{cm}^{\prime}}{l_{cr}^{\prime}}\psi_{cr}^{\prime} - \frac{p_p l_{cm}^{\prime}}{l_{cr}^{\prime}}\overline{\psi}_{ps}^{m}\right)i_{cs}^{t} + \frac{p_p l_{cm}^{\prime}}{l_{cr}^{\prime}}\overline{\psi}_{ps}^{t}i_{cs}^{m} \tag{17}$$

The expected values of the CM rotor flux and torque are substituted into (15)–(17), and the reference values of the CM stator current and the slip velocity in the rotor field-oriented m-t reference frame are calculated by using the inverse model. The torque and the CM rotor flux are replaced by a given value, and the m-t reference frame synchronous angle is obtained by calculating the slip frequency integral plus the rotor position. The other variables are the measured values of the m-t reference frame. The expression is as follows:

$$i_{cs}^{m*} = \frac{1}{l_{cm}^{\prime}}\psi_{cr}^{\prime\ *} + \frac{l_{cr}^{\prime}}{l_{cm}^{\prime}\left(r^{\prime}{}_r + r_{ps}\right)}\left(\overline{u}_{ps}^{m} - p_p\omega_r\overline{\psi}_{ps}^{t}\right) - \frac{l_{cr}^{\prime}r_{ps}}{l_{cm}^{\prime}l_{ps}\left(r^{\prime}{}_r + r_{ps}\right)}\overline{\psi}_{ps}^{m} \tag{18}$$

$$\dot{\lambda}^{*} = \frac{-p_p\omega_r\overline{\psi}_{ps}^{m} + \frac{r_{ps}}{l_{ps}}\overline{\psi}_{ps}^{t} - \overline{u}_{ps}^{t} + \frac{\left(r_r^{\prime}+r_{ps}\right)l_{cm}^{\prime}}{l_{cr}^{\prime}}\psi_{cr}^{\prime\ *}}{\psi_{cr}^{\prime\ *}} \tag{19}$$

$$i_{cs}^{t*} = \frac{T_e^{*} - \frac{p_p l_{cm}^{\prime}}{l_{cr}^{\prime}}\overline{\psi}_{ps}^{t}i_{cs}^{m*} + \frac{p_p}{l_{cr}^{\prime}}\overline{\psi}_{ps}^{t}\psi_{cr}^{\prime\ *}}{\frac{l_{cm}^{\prime}}{l_{cr}^{\prime}}\left(p_c\psi_{cr}^{\prime\ *} - p_p\overline{\psi}_{ps}^{m}\right)} \tag{20}$$

Figure 4 shows the BDFM slip frequency vector feedback linearization control (SFV-FLC) block diagram. First, the excitation current and torque current are calculated by giving the CM rotor flux and the electromagnetic torque. The torque reference value is obtained by the speed PI regulator. The known CM rotor flux and excitation current in (18) and (20) are substituted into (19) to calculate the slip velocity, so indirect magnetic field orientation is realized. Secondly, the difference between the reference current and the actual current, and the control voltage under the m-t reference frame, is obtained by the PI regulator, which is transformed into a three-phase static reference frame. Finally, the BDFM is controlled by SPWM modulation.

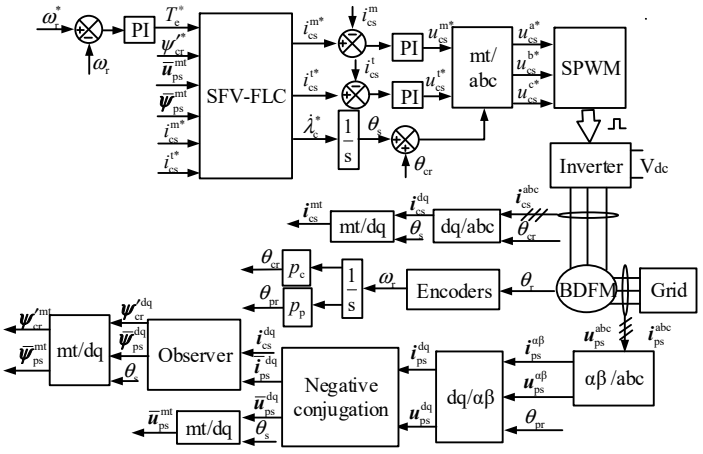

Figure 4. BDFM slip frequency vector feedback linearization control (SFV-FLC) block diagram.

$p_c{\psi'}^*_{cr} - p_p\overline{\psi}^m_{ps}$ is shown in the denominator position of the electromagnetic torque expression (20). $p_c{\psi'}^*_{cr} - p_p\overline{\psi}^m_{ps}$ is not to be zero; otherwise, this control cannot be realized. The necessary conditions for the solution of the SFV-FLC are obtained, namely,

$$p_c{\psi'_{cr}}^* - p_p\overline{\psi}^m_{ps} \neq 0 \text{ and } {\psi'_{cr}}^* > \frac{p_p}{p_c}\overline{\psi}^m_{ps} \tag{21}$$

When the PM stator is open circuit, that is, $\overline{\psi}^t_{ps} = \overline{\psi}^m_{ps} = \overline{u}^t_{ps} = \overline{u}^m_{ps} = 0$ in (18)–(20), then the SFV control law of the induction motor can be obtained.

5. Performance Analysis

According to the CM's rotor field orientation, the load characteristics of the BDFM slip frequency vector feedback linearization control system are discussed below when the PM is supplied with constant voltage and frequency.

When the machine is running in a steady state, the state variables in (11) become DC values, the derivative of the PM stator flux and the CM rotor flux become zero, and the static equation of BDFM can be written as follows:

$$0 = \left(-\frac{r_{ps}}{l_{ps}} + j\left(p_p\omega_r - \dot{\lambda}\right)\right)\overline{\psi}^{mt}_{ps} + \frac{r_{ps}}{l'_{cr}}\psi'_{cr} + \overline{u}^{mt}_{ps} - \frac{r_{ps}l'_{cm}}{l'_{cr}}i^{mt}_{cs} \tag{22}$$

$$0 = \left(\frac{r_{ps}}{l_{ps}} - jp_p\omega_r\right)\overline{\psi}^{mt}_{ps} + \frac{(r'_r + r_{ps})l'_{cm}}{l'_{cr}}i^{mt}_{cs} - \overline{u}^{mt}_{ps} - \left(\frac{(r'_r + r_{ps})}{l'_{cr}} + j\dot{\lambda}\right)\psi'_{cr} \tag{23}$$

The Equations (22) and (23) are combined to eliminate the PM stator voltage, and the expressions for the CM stator current, the PM stator flux and the CM rotor flux are obtained:

$$i^{mt}_{cs} = \left(\frac{1}{l'_{cm}} + j\frac{\dot{\lambda}l'_{cr}}{r'_r l'_{cm}}\right)\psi'_{cr} + j\frac{\dot{\lambda}l'_{cr}}{r'_r l'_{cm}}\overline{\psi}^{mt}_{ps} \tag{24}$$

The Equation (24) is substituted into (22), and the CM stator current is eliminated to obtain the following:

$$\overline{u}^{mt}_{ps} = \left(\frac{r_{ps}}{l_{ps}} + j\left(\frac{\dot{\lambda}r_{ps}}{r'_r} - \left(p_p\omega_r - \dot{\lambda}\right)\right)\right)\overline{\psi}^{mt}_{ps} + j\frac{\dot{\lambda}r_{ps}}{r'_r}\psi'_{cr} \tag{25}$$

The PM is connected to the constant voltage and frequency power grid (220 V/50 Hz). The voltage amplitude and frequency are constant. That is, the PM supply constraint is as follows:

$$\begin{cases} \omega_p = 2\pi f_p = p_p\omega_r - \dot{\lambda} \\ \overline{u}^2_{ps} = \left(\overline{u}^m_{ps}\right)^2 + \left(\overline{u}^t_{ps}\right)^2 \end{cases} \tag{26}$$

Multiply the two sides of (25) by their conjugations, and then combine with (26) to obtain,

$$\overline{u}^2_{ps} = \left(b_1^2 + b_2^2\right)\overline{\psi}^2_{ps} + 2b_3\mathrm{Re}\left\{(b_2 - jb_1)\overline{\psi}^{mt}_{ps}\psi'_{cr}\right\} + {b_3}^2{\psi'_{cr}}^2 \tag{27}$$

where $\overline{\psi}^2_{ps} = \overline{\psi}^{m2}_{ps} + \overline{\psi}^{t2}_{ps}$, $b_1 = r_{ps}/l_{ps}$, $b_2 = \dot{\lambda}r_{ps}/r'_r - \left(p_p\omega_r - \dot{\lambda}\right)$, $b_3 = \dot{\lambda}r_{ps}/r'_r$.

Equation (24) is substituted into (12) to obtain the electromagnetic torque equation,

$$T_e = \frac{\dot{\lambda}}{r'_r}\left(-p_p\overline{\psi}^2_{ps} + p_c{\psi'_{cr}}^2 + (p_c - p_p)\psi'_{cr}\overline{\psi}^m_{ps}\right) \tag{28}$$

It can be seen from (28) that $\dot{\lambda}/r'_{\mathrm{r}}$ is constant when slip velocity and machine parameters are fixed. Based on the above conditions, the torque boundary corresponding to the BDFM sinusoidal steady-state solution can be reached when $\overline{\psi}^{\mathrm{m}}_{\mathrm{ps}} = -\overline{\psi}_{\mathrm{ps}}$ or $\overline{\psi}^{\mathrm{m}}_{\mathrm{ps}} = \overline{\psi}_{\mathrm{ps}}$.

The PM's stator flux amplitude is affected by the stator current's voltage drop on the stator resistance. To calculate the BDFM output torque boundary, the PM voltage Equation (27) and torque Equation (28) are simultaneous equations. The electromagnetic torque equals the load torque when the machine is in a steady state. To derive the quadratic equation for the PM stator flux,

$$\frac{a_1k_2^2 + a_1k_1^2}{k_2^2}\left(\overline{\psi}^{\mathrm{m}}_{\mathrm{ps}}\right)^2 + \frac{2a_1k_1\,k_3 + a_2k_2^2\psi'_{\mathrm{cr}}}{k_2^2}\overline{\psi}^{\mathrm{m}}_{\mathrm{ps}} + \frac{a_1k_3^2}{k_2^2} + a_3{\psi'_{\mathrm{cr}}}^2 - T_{\mathrm{L}} = 0 \tag{29}$$

where,

$$k_1 = a_2\left(b_1^2 + b_2^2\right)\psi'_{\mathrm{cr}} - 2a_1b_2b_3\psi'_{\mathrm{cr}}, k_3 = -\left(b_1^2 + b_2^2\right)T_{\mathrm{L}} + a_1\overline{u}^2_{\mathrm{ps}} + \left(a_3\left(b_1^2 + b_2^2\right) - a_1b_3^2\right){\psi'_{\mathrm{cr}}}^2$$

$$k_2 = 2a_1b_1b_3\psi'_{\mathrm{cr}}, a_1 = -p_{\mathrm{p}}\dot{\lambda}/r'_{\mathrm{r}}, a_2 = -\left(p_{\mathrm{p}} - p_{\mathrm{c}}\right)\dot{\lambda}/r'_{\mathrm{r}}, a_3 = p_{\mathrm{c}}\dot{\lambda}/r'_{\mathrm{r}}.$$

As seen from (25), when the PM stator voltage is constant, given the CM rotor flux, slip velocity, and load torque, the PM's stator flux solution can be obtained. When the load torque gradually increases and gradually decreases, (29) is not the real solution. In this case, the BDFM has reached the torque boundary. According to the BDFM parameters in Table 1, the load boundaries of the BDFM are calculated by MATLAB, as shown in Figure 5. To facilitate understanding, convert the above 3D surface into 2D, as shown in Figure 6. The load torque in the figure is expressed in per unit value, $T_{\mathrm{Lb}} = T_{\mathrm{L}}/T_N$.

Table 1. BDFM Experimental parameters.

Parameter	Value	Parameter	Value
P(KW)	8	$r_{\mathrm{ps}}/r_{\mathrm{cs}}$ (Ω)	0.813/0.533
T_{N}/(N·m)	50	$r_{\mathrm{pr}}/r_{\mathrm{cr}}$ (Ω)	0.6/0.493
p_{p}	1	$l_{\mathrm{ps}}/l_{\mathrm{cs}}$ (H)	0.372/0.0649
p_{c}	3	$l_{\mathrm{pm}}/l_{\mathrm{cm}}$ (H)	0.367/0.0636

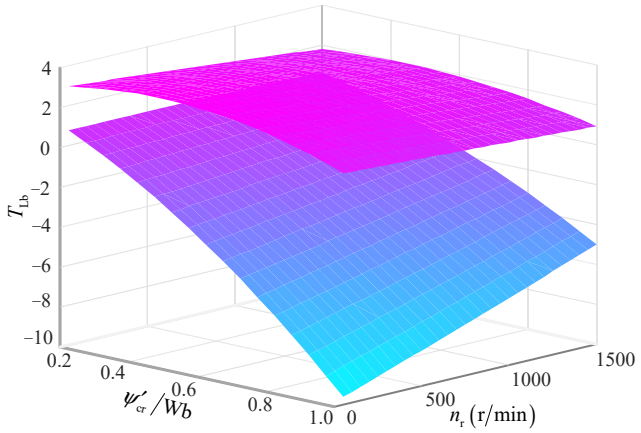

Figure 5. The boundaries of load torque.

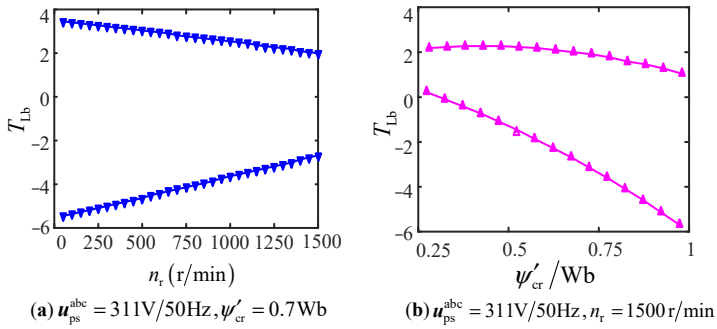

Figure 6. The bounds of the load torque when speed and CM rotor flux vary.

Figure 5 shows that the load torque of the BDFM with steady-state sinusoidal solution has a boundary. Under the condition that the stator voltage and the PM's supply frequency are fixed, the BDFM output torque boundary varies with the CM rotor flux and the machine speed. However, the load boundaries of the BDFM are not symmetrical. When the CM rotor flux amplitude is greater than a specific value, the upper bound of output torque will be less than zero. When the CM rotor flux amplitude is less than a specific value, the lower bound of output torque will be greater than zero.

Figure 6a shows that when the CM rotor flux ψ'_{cr} = 0.7 Wb, the static load-interval width decreases from sub-synchronous to synchronous to super-synchronous (The synchronous speed is 750 r/min), and the load capacity is weakened; the load torque boundaries are shown in Table 2. Figure 6b shows that when the speed n_r = 1500 r/min, the load-interval width becomes more extensive with the rotor flux amplitude increase, but the machine's positive load capacity becomes weaker. Therefore, when the machine is running at high speed, the load capacity can be improved by reducing the CM rotor flux. Unless the slip frequency is particularly low, reducing the CM rotor flux can always cause the machine torque to be much higher than the rated value.

Table 2. The boundaries of load torque at ψ'_{cr} = 0.7 Wb.

n_r (r/min)	$\dot{\lambda}$ (r/min)	T_{Lb}
300	−2700	[3.49, −5.24]
600	−2400	[3.12, −4.58]
900	−2100	[2.74, −3.91]
1200	−1800	[2.37, −3.25]
1500	−1500	[2.00, −2.59]

When the PM stator resistance is minimal and the PM stator flux is kept constant, the torque Equation (28) is linearly related to the rotor resistance and slip velocity under the specific CM rotor flux. Figure 7 shows the boundaries of the BDFM loaded interval before and after the rotor resistance reduction by 0.5 times, calculated by MATLAB. To facilitate understanding, convert the 3D surface to 2D, and the result is shown in Figure 8.

From Figure 8 and Table 3, when ψ'_{cr} = 0.7 Wb, the load torque boundaries are proportional to the slip velocity and inversely proportional to the rotor resistance. When the slip velocity is constant, the load torque boundaries are inversely proportional to the rotor resistance. When the rotor resistance is minimal and the rotor loss can be neglected, the CM torque and PM torque are controlled in the same direction. The ratio of the two-machine torque is equal to the ratio of the pole-pairs number of the two machines.

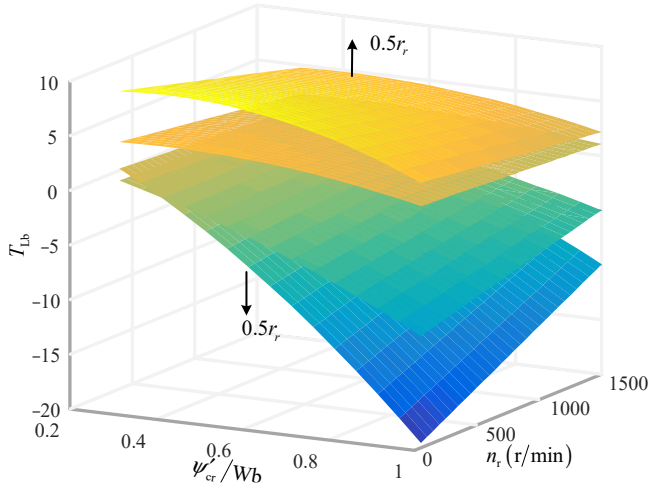

Figure 7. The bounds of the load torque when the PM stator resistance is negligible.

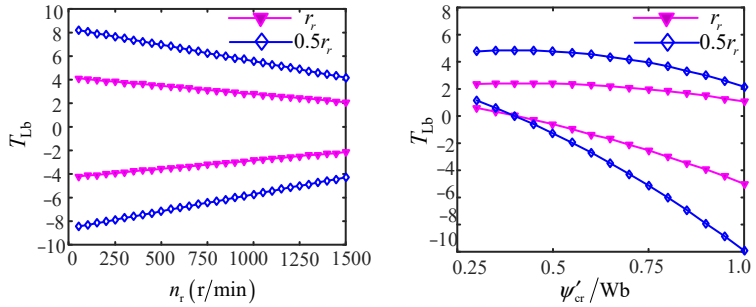

Figure 8. The bounds of the load torque when speed and CM rotor flux vary.

Table 3. The boundaries of load torque at ψ'_{cr} = 0.7 Wb.

n_r (r/min)	$\dot{\lambda}$ (r/min)	T_{Lb}	
		r_r	$0.5r_r$
300	−2700	[3.76, −3.84]	[7.52, −7.72]
600	−2400	[3.36, −3.44]	[6.68, −6.88]
900	−2100	[2.92, −3.00]	[5.84, −6.00]
1200	−1800	[2.52, −2.56]	[5.04, −5.12]
1500	−1500	[2.08, −2.12]	[4.16, −4.28]

6. Simulation Results

To verify the effectiveness of the research content proposed in the paper, the BDFM control system model is established based on MATLAB /Simulink. In the simulation and experiment, the CM is powered by the inverter, and the Siemens inverter powers the PM. The Siemens inverter is powered by 44 V/10 Hz. The inverter's DC voltage is 150 V. As can be seen in (18), (19), and (20), it is necessary to observe the machine flux during the control process. Therefore, the rotor voltage equation in (6) and the rotor flux equation in (9) are combined to eliminate the rotor current, and the flux observation model in the d-q reference frame is obtained:

$$\begin{cases} \overline{\psi}_{ps}^{dq} = -\frac{l'_{pm}l'_{cm}s}{(r'_r+l'_rs)}\dot{i}_{cs}^{dq} + \frac{l_{ps}(r'_r+l'_{cr}s)}{(r'_r+l'_rs)}\bar{i}_{ps}^{dq} \\ \psi'^{\,dq}_{cr} = \frac{l'_{cm}(r'_r+l'_{pm}s)}{(r'_r+l'_rs)}\dot{i}_{cs}^{dq} - \frac{l'_{cr}l'_{pm}s}{(r'_r+l'_rs)}\bar{i}_{ps}^{dq} \end{cases} \quad (30)$$

Of course, the PM's stator flux can also be obtained by using the voltage and current model in the static reference frame. The PM stator flux linkage is obtained by using the large inertia instead of pure integration to solve the problem of DC offset.

6.1. Verification of Decoupling Performance

The CM rotor flux reference value is 0.45 Wb. Combining with (29) and Table 1, the results show that when the rotor speed changes from 75 r/min to 225 r/min, the positive boundary of the load changes from 13.2 N.m to 10.7 N.m, and the negative boundary of the load changes from −38. 4 N.m to −28.5 N.m. The rotor speed loop is added in the simulation and experiment based on the SFV-FLC. When the reference speed is from 75 r/min to 150 r/min to 225 r/min; the step increase speed, step decrease speed, and torque limit are ±10 N.m; the simulation results are shown in Figure 9. When the reference speed (synchronous speed) is 150 r/min and the load torque is 8 N.m, the simulation results are shown in Figure 10. When the reference speed is 75 r/min and the load torque is 8 N.m, the simulation results are shown in Figure 11. When the reference speed is changed from 150 r/min to 75 r/min, and the torque limit is ± 20 N.m, the simulation results are shown in Figure 12. When the reference speed is an under-synchronous speed of 75 r/min, and step load torque is applied from no-load to 10 N.m, the simulation results are shown in Figure 13.

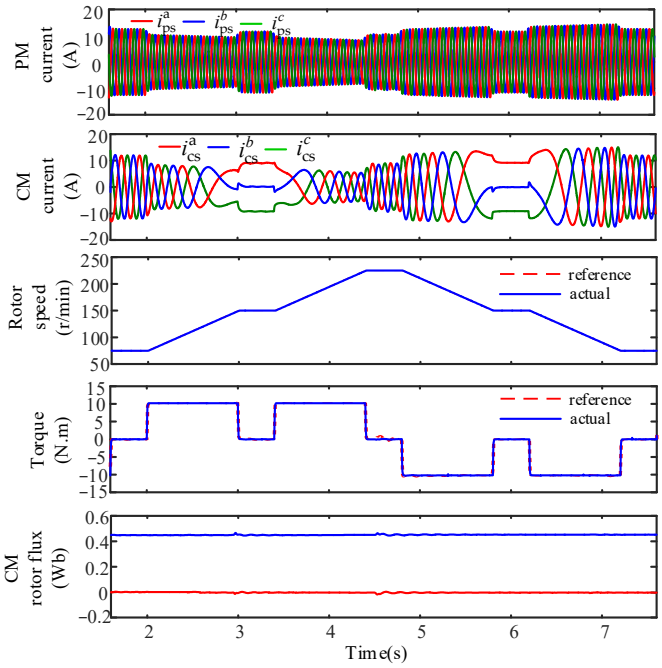

Figure 9. Simulation results of step increase and decrease.

As shown in Figure 9, the rotor speed and the CM rotor flux can accurately track the reference value. In increasing speed and decreasing speed, the torque change does not affect the CM rotor flux. The results show that the decoupling control method can eliminate the coupling effect between the flux and torque and realize high-performance decoupling control. In addition, the CM stator current waveform shows that 150 r/min is the synchronous speed. The CM's stator phase sequence changes when the synchronous speed runs up and down. When the rotor speed increases from 75 r/min to 225 r/min in 2 s~4.8 s, the CM changes from a negative phase sequence to a positive phase sequence, and the machine runs in the super-synchronous state. When the rotor speed decreases from 225 r/min to 75 r/min in 4.8 s~7.6 s, the CM changes from a positive phase sequence to a negative phase sequence and the machine runs in an under-synchronous state.

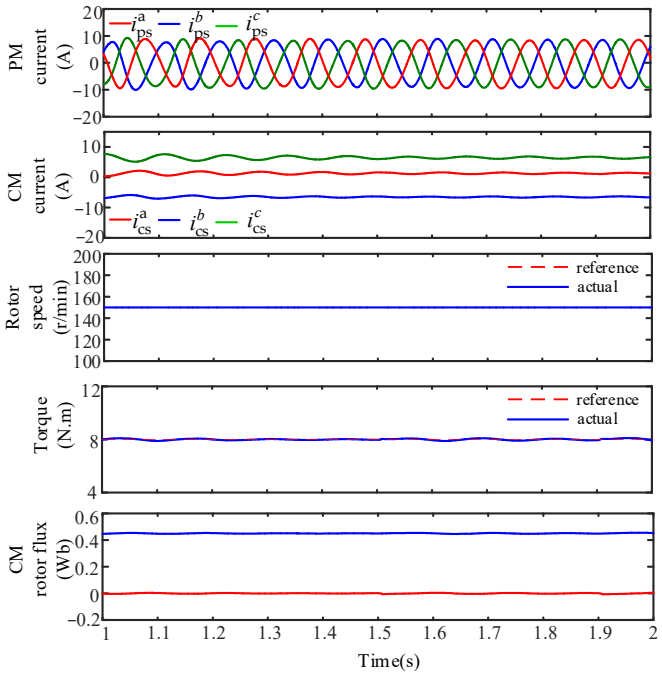

Figure 10. Simulation results at a synchronous speed of 150 r/min.

As shown in Figure 10, the load torque is 8 N.m. The rotor speed is stable at a synchronous speed of 150 r/min (the CM power supply frequency is 0). The CM rotor flux and the rotor speed are controlled to track the reference value accurately.

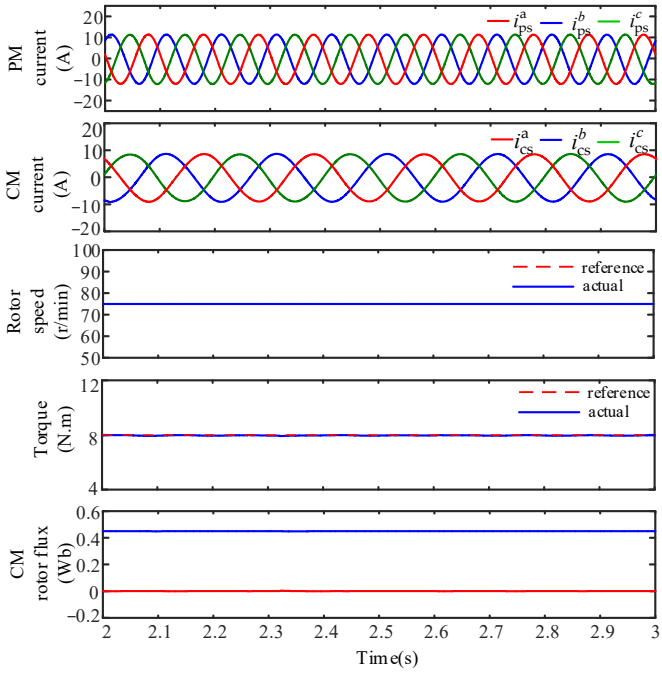

Figure 11. Simulation results of under-synchronization at 75 r/min.

As shown in Figure 11, the load torque is 8 N.m. The rotor speed is stable at an under-synchronous speed of 75 r/min (the negative phase sequence of the CM power supply output and power supply frequency is 5 Hz). The CM rotor flux and the rotor speed are controlled to track the reference value accurately.

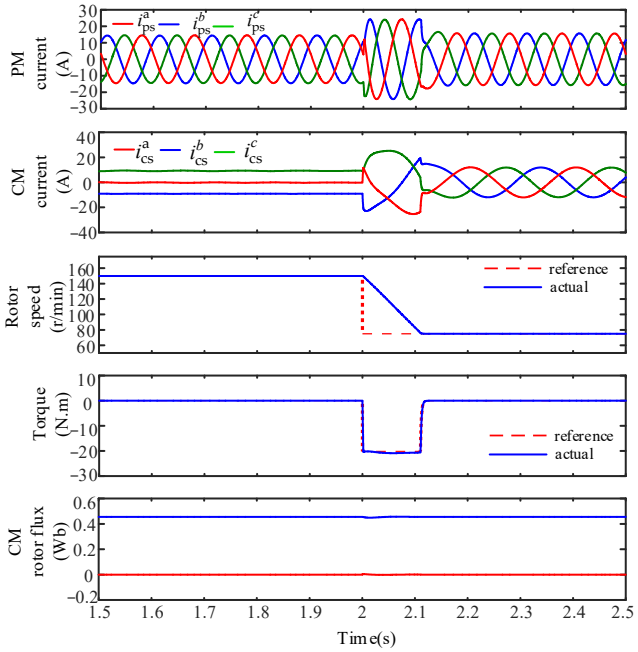

Figure 12. Simulation results with step change of speed.

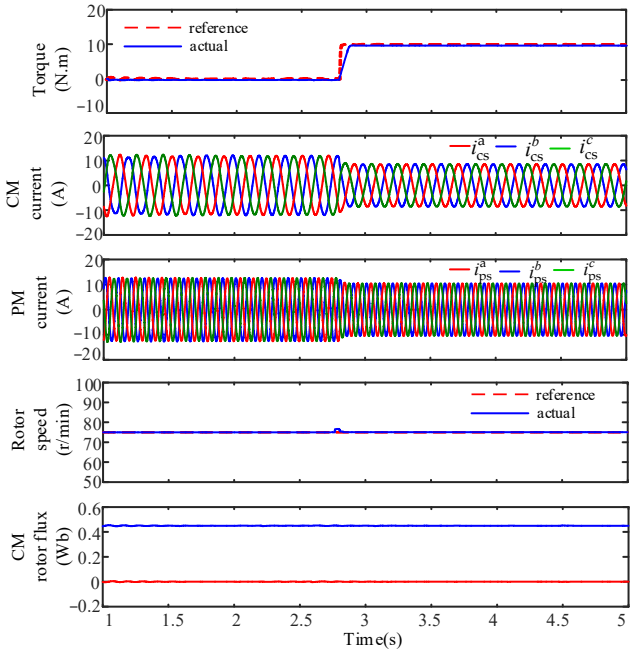

Figure 13. Simulation results when step disturbance is applied.

As depicted in Figure 12, the rotor speed changes from 150 r/min to 75 r/min at 2 s, the CM frequency changes from 0 to the negative phase sequence 5 Hz, and the rotor speed responds quickly and is stable at the reference value. When the rotor speed step changes, the CM rotor flux is stable at the reference value. In addition, the system has a stable output torque of −20 N.m in 2 s~2.12 s; the rotor speed enters the steady state, and the torque is immediately stable at 0 N.m in 2.12 s~2.5 s. The results show that the control strategy is effective.

As depicted in Figure 13, the reference speed of 75 r/min is kept constant, at which point the CM power supply frequency is the negative phase sequence 5 Hz. When 10 N.m load torque is added at 2.8 s, the torque response is fast, and the reference value is tracked accurately. With the increase in load torque, the CM and PM stator current decrease. When

the load torque changes suddenly, the rotor flux is stable at the reference. Simulation results show that the strategy has anti-load disturbance performance.

6.2. Verification of Load Boundary

The CM rotor flux reference value is 0.45 Wb. The combined (31) and Table 1 calculated that when the rotor speed is 75 r/min, the positive and negative load boundaries are 13.2 N.m and −38.4 N.m, respectively. In this paper, only the positive load boundary is verified. In the simulation, the load torque from 10 N.m increases gradually.

From Figure 14, the rotor speed and rotor flux do not change with the increase in torque in 1 s~2.5 s, so the decoupling of flux and torque is realized. The load torque applied exceeds the load positive boundary 13.2 N.m in 2 s~4 s. The CM and PM' stator current waveforms are non-sinusoidal, and the flux and torque fluctuate greatly. The control strategy presented in the paper loses decoupling and dynamic tracking characteristics. The simulation results show that the loaded boundary is effective.

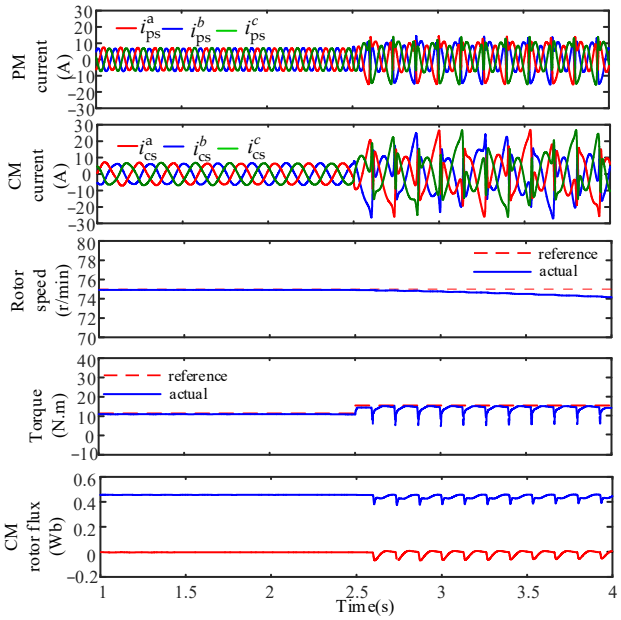

Figure 14. Simulation results of load boundary verification.

7. Experimental Results

The BDFM experimental platform, as shown in Figure 15, is built in the laboratory.

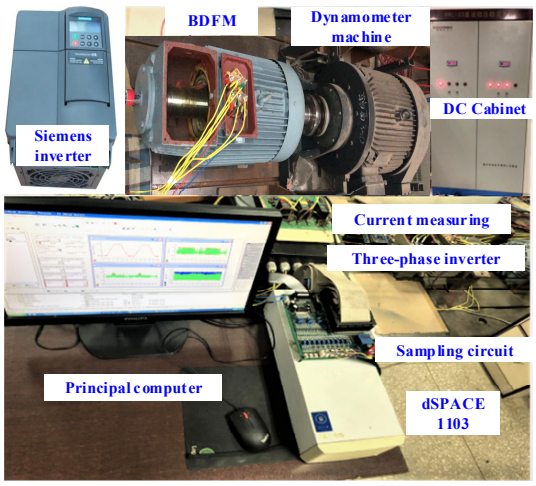

Figure 15. BDFM experimental platform.

Figure 16 shows the hardware platform connection diagram. This mainly includes the BDFM, the DC Cabinet, the Siemens Inverter, the dynamometer machine, the inverter, the control algorithm by dSPACE hardware in the loop system, and Matlab/Simulink modeling real-time interface (RTI) automatically compiles and downloads to dSPACE 1103 control board to achieve.

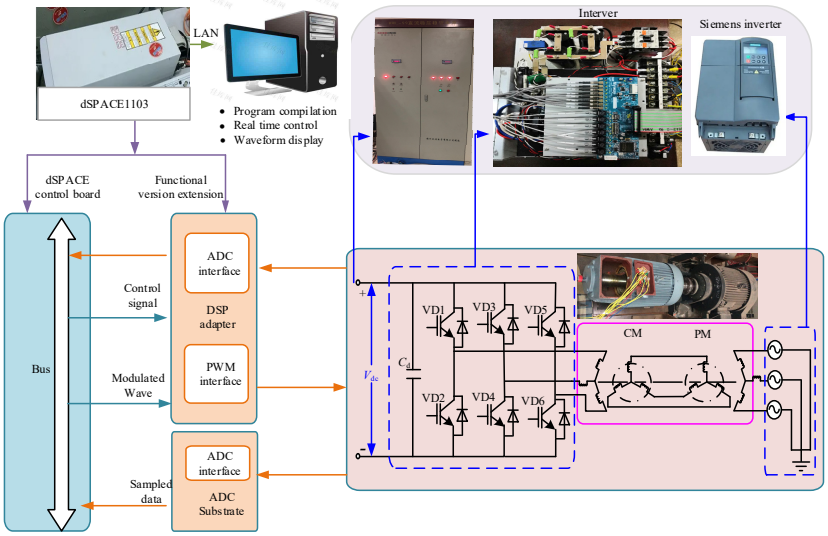

Figure 16. Hardware experimental platform connection diagram.

7.1. Verification of Decoupling Performance

The dynamic tracking and decoupling performance of the BDFM are tested under the same simulation conditions as in Section 6.

As depicted in Figure 17, the rotor speed and the CM rotor flux can accurately track the reference value. In increasing and decreasing speed, the torque change does not affect the CM rotor flux. The results show that the decoupling control method can eliminate the coupling effect between the flux and the torque and realize high-performance decoupling control. In addition, the CM stator current waveform shows that the rotor speed increases from 75 r/min to 225 r/min in 1.5 s~3 s, the CM changes from a negative phase sequence to a positive phase sequence, and the machine runs in the super-synchronous state. The rotor speed decreases from 225 r/min to 75 r/min in 4.5 s~7.2 s, the CM changes from a positive phase sequence to a negative phase sequence, and the machine runs in an under-synchronous state.

As depicted in Figure 18, the applied load torque is 8 N.m. The rotor speed is stable at a synchronous speed of 150 r/min (the CM power supply frequency is 0 Hz). The CM rotor flux and the rotor speed are controlled to track the reference value accurately. Experimental results show that the control strategy has a good response performance.

As depicted in Figure 19, the applied load torque is 8 N.m. The rotor speed is stable at an under-synchronous speed of 75 r/min (the CM power supply frequency is the negative phase sequence 5 Hz). The CM phase sequence is opposite to the PM phase sequence. The CM rotor flux and the rotor speed are controlled to track the reference value accurately. The results further verify the feasibility of the control method.

From Figure 20, the rotor speed changes from 150 r/min to 75 r/min at 1.9 s, the control frequency changes from 0 to the negative phase sequence 5 Hz, and the rotor speed responds quickly and is stable at the reference value. When the rotor speed step changes, the CM rotor flux does not change with the torque change, and the precise decoupling of the flux and the torque is realized. In addition, the system has a stable output torque of −20 N.m in 1.9 s~2.1 s; the rotor speed enters the steady state, and the torque is immediately stable at 0 N.m in 2.2 s~2.5 s. The experimental results present that the control strategy has good decoupling performance.

From Figure 21, the reference speed of 75 r/min is kept constant, at which point the CM power supply frequency is the negative phase sequence 5 Hz. When adding 10 N.m load torque at 2.8 s, the torque response is fast, and the reference value is tracked accurately. The CM and PM stator current decrease with the increase in load torque. When the load torque changes suddenly, the rotor flux keeps constant, and the decoupling of flux and torque is realized. The experimental results are consistent with the simulation results and show that the strategy has good control and anti-load disturbance performance.

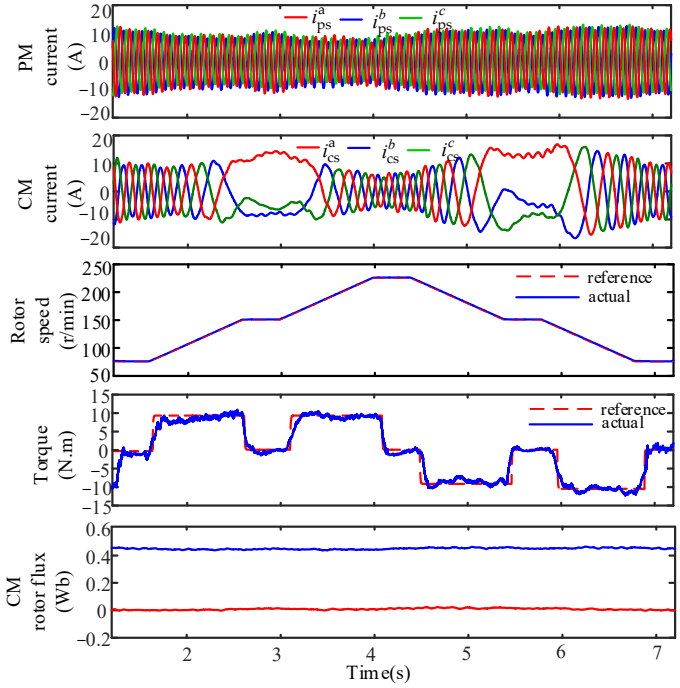

Figure 17. Experimental results of step increase speed and step decrease speed.

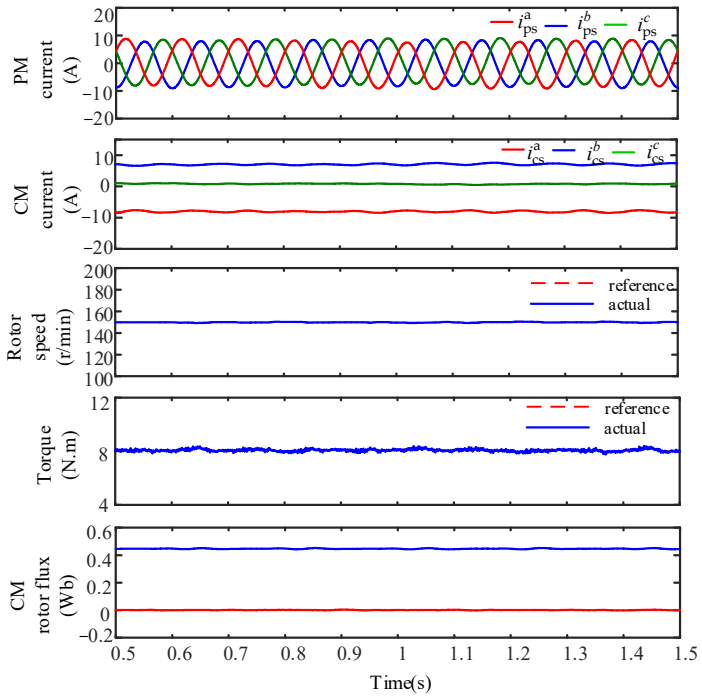

Figure 18. Experimental results at a synchronous speed of 150 r/min.

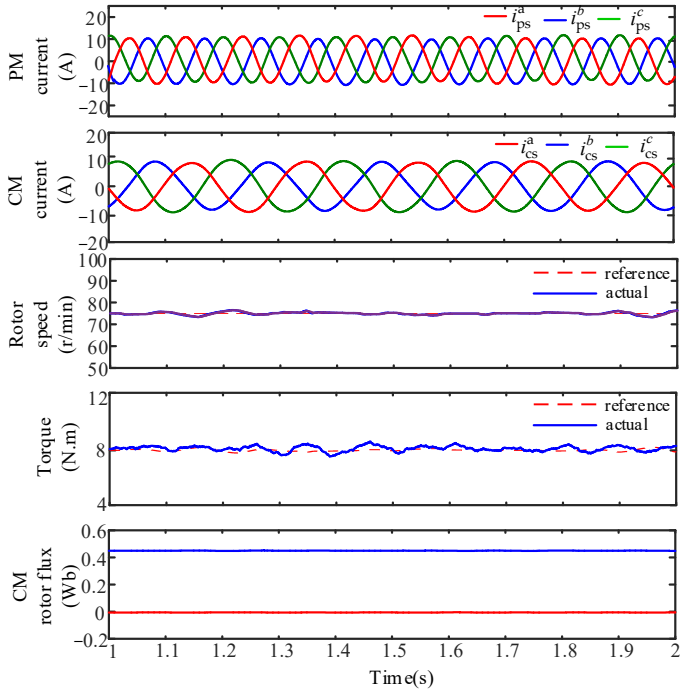

Figure 19. Experimental results of under-synchronization at 75 r/min.

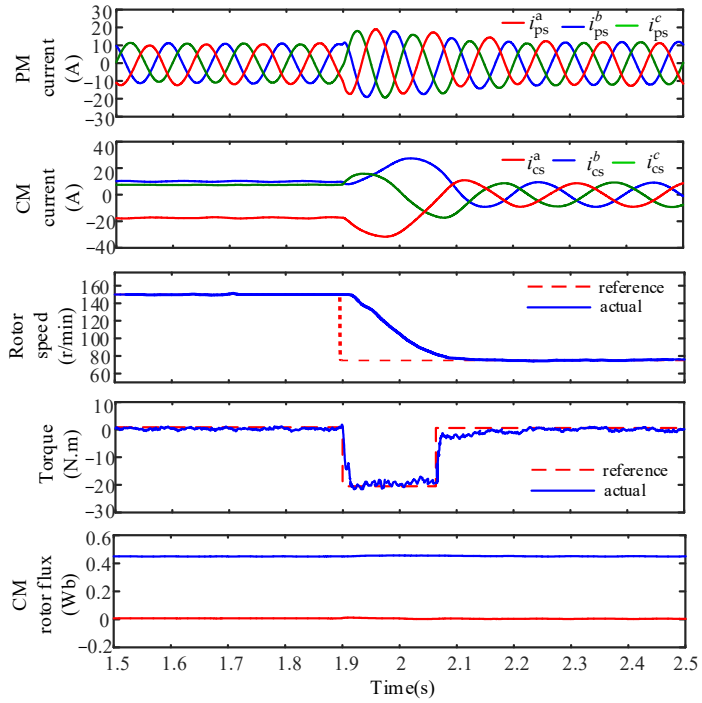

Figure 20. Experimental results with step change of speed.

7.2. Verification of Load Boundary

The same simulation conditions as in Section 6 are selected to verify the positive load boundary with the BDFM.

From Figure 22, the rotor speed and rotor flux are unaffected by an increase in torque. in 1 s~2.5 s, so the flux and torque become decoupled. The load torque applied exceeds the load positive boundary 13.2 N.m in 2.5 s~4 s. The CM and PM stator current is non-sinusoidal, and the flux and torque fluctuate considerably. The control strategy presented in the paper loses decoupling and dynamic tracking characteristics. The results present that the performance analysis is effective.

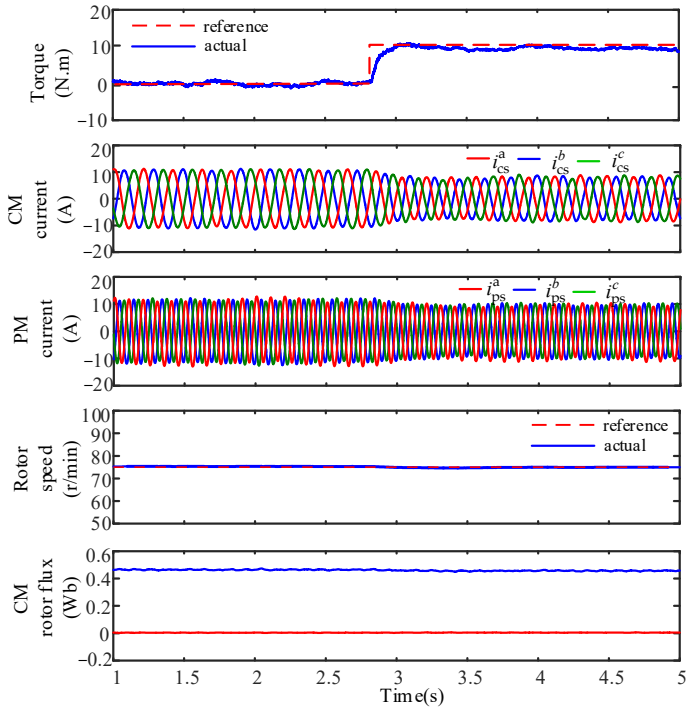

Figure 21. Experimental results when step disturbance is applied.

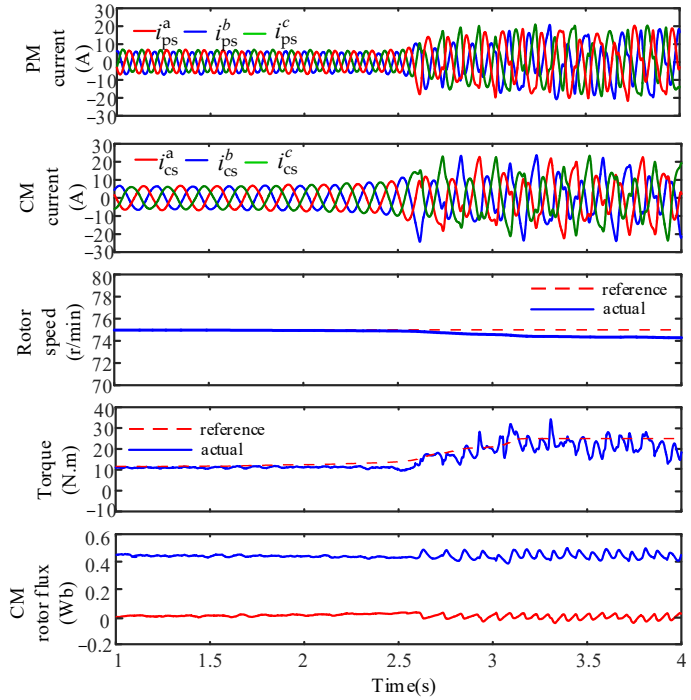

Figure 22. Experimental results of load boundary verification.

By comparing the simulation results in Figures 9–14 with the experimental results in Figures 17–22, it can be seen that when the simulation conditions are consistent with the experimental conditions, the conclusions of the simulation and the experiment are consistent, but there is a slight difference between the two waveforms. Since the voltage and current sampling in the simulation are in an ideal condition, there is no interference from external factors. In the experiment, the voltage and current are sampled through the sensor. Due to the interference of various factors, the sampling signal will have weak ripples, which will affect the feedback control, the observation of the actual torque, and

the observation of the rotor flux. Therefore, the control effect of each variable observed in the experimental results is slightly different from that in the simulation, but the verified conclusions are consistent. If the BDFM runs within the load boundary, the SFV-FLC can realize the decoupling of the flux linkage and torque. If the torque boundary is exceeded, the whole system loses its decoupling characteristics.

8. Conclusions

This paper presents the slip frequency vector feedback linearization control (SFV-FLC) strategies and analyses the BDFM control performance under supply constraints. Its contribution lies in the SFV-FLC method that can realize the effective decoupling of the CM rotor flux and the torque. In addition, the BDFM control characteristics analysis shows that when neglecting the PM stator resistance, the BDFM load boundary is inversely proportional to the rotor resistance and directly proportional to the slip velocity. Theoretical derivation and experimental results prove the feasibility and correctness of the control strategy and performance analysis. The research presented in the study applies to the squirrel-cage BDFM. These results are not only beneficial to the machine system design but also help to reduce the fault [31] rate of the machine operation.

Author Contributions: Conceptualization, C.X.; methodology, C.X.; software, C.X. and N.W.; validation, C.X. and N.W.; formal analysis, C.X.; investigation, C.X.; resources, C.X.; data curation, C.X; writing—original draft preparation, C.X. and N.W.; writing—review and editing, C.X. and N.W.; visualization, C.X. and N.W.; supervision, C.X.; project administration, C.X.; funding acquisition, C.X. All authors have read and agreed to the published version of the manuscript.

Funding: This research received no external funding.

Data Availability Statement: All the data are shown in the tables and figures of this paper.

Conflicts of Interest: The authors declare no conflict of interest.

References

1. Wang, X.Z.; Strous, T.D.; Lahaye, D.; Polinder, H.; Ferreira, J.A. Modeling and Optimization of Brushless Doubly-Fed Induction Machines Using Computationally Efficient Finite-Element Analysis. *IEEE Trans. Ind. Appl.* **2016**, *52*, 4525–4534. [CrossRef]
2. Han, P.; Cheng, M.; Jiang, Y.L.; Chen, Z. Torque/Power Density Optimization of a Dual-Stator Brushless Doubly-Fed Induction Generator for Wind Power Application. *IEEE Trans. Ind. Electron.* **2017**, *64*, 9864–9875. [CrossRef]
3. Agrawal, S.; Province, A.; Banerjee, A. An Approach to Maximize Torque Density in a Brushless Doubly Fed Reluctance Machine. *IEEE Trans. Ind. Appl.* **2020**, *56*, 4829–4838. [CrossRef]
4. Han, P.; Zhang, J.; Cheng, M. Analytical Analysis and Performance Characterization of Brushless Doubly Fed Machines With Multi-barrier Rotors. *IEEE Trans. Ind. Appl.* **2019**, *55*, 5758–5767. [CrossRef]
5. Mathekga, M.E.; Ademi, S.; McMahon, R.A. Brushless Doubly Fed Machine Magnetic Field Distribution Characteristics and Their Impact on the Analysis and Design. *IEEE Trans. Energy Convers.* **2019**, *34*, 2180–2188. [CrossRef]
6. Zhang, F.; Yu, S.Y.; Wang, Y.T.; Jin, S.; Jovanovic, M.G. Design and Performance Comparisons of Brushless Doubly Fed Generators With Different Rotor Structures. *IEEE Trans. Ind. Electron.* **2019**, *66*, 631–640. [CrossRef]
7. Oraee, A.; McMahon, R.; Abdi, E.; Abdi, S.; Ademi, S. Influence of Pole-Pair Combinations on the Characteristics of the Brushless Doubly Fed Induction Generator. *IEEE Trans. Energy Convers.* **2020**, *35*, 1151–1159. [CrossRef]
8. Chen, H.T.; Li, L.L.; Shang, C.; Huang, B. Fault Detection for Nonlinear Dynamic Systems With Consideration of Modeling Errors: A Data-Driven Approach. *IEEE Trans. Cybern.* **2022**, 1–11. [CrossRef]
9. Olubamiwa, O.I.; Hutton, T.; Gule, N. Brushless Doubly Fed Machine Design Evaluation with Power Factor Considerations. *IEEE Trans. Ind. Appl.* **2022**, 1–12. [CrossRef]
10. Pan, W.; Yu, K.; Chen, X.; Wang, X.; Xie, X. Design of a Wound Rotor Brushless Doubly-Fed Machine With 1/5 Pole-Pair Combination. *IEEE Trans. Ind. Electron.* **2022**, 1–11. [CrossRef]
11. Cheng, Y.; Yu, B.; Wang, X. Rotor Winding Design and Standalone Operation Research of High Natural Synchronous Speed Brushless Doubly-Fed Generator Based on Differential Modulation. *IEEE Trans. Ind. Electron.* **2022**, 1–9. [CrossRef]
12. Chen, X.; Wang, X.; Kong, M.; Li, Z. Design of a Medium-Voltage High-Power Brushless Doubly Fed Motor With a Low-Voltage Fractional Convertor for the Circulation Pump Adjustable Speed Drive. *IEEE Trans. Ind. Electron.* **2022**, *69*, 7720–7732. [CrossRef]
13. Kan, C.; Jiang, T.; Jin, K.; Fang, Y.; Zhang, H. Soft-starting Brushless Doubly Fed Machine Winding design and Magnetic Field Analysis. *IEEE Trans. Ind. Appl.* **2022**, 1–9. [CrossRef]
14. Chen, H.T.; Liu, Z.G.; Alippi, C.; Huang, B.; Liu, D.R. Explainable Intelligent Fault Diagnosis for Nonlinear Dynamic Systems: From Unsupervised to Supervised Learning. *IEEE Trans. Neural Netw. Learn. Syst.* **2022**, 1–14. [CrossRef]

15. Li, Y.; Lu, N.Y.; Jiang, B.; Ma, Y.J.; Wang, X.L. An islanding fault detection method with CFDF-SVM based RPV approach under pseudo islanding phenomenon. In Proceedings of the 10th International-Federation-of-Automatic-Control (IFAC) Symposium on Fault Detection, Supervision and Safety for Technical Processes, Warsaw, Poland, 29–31 August 2018. [CrossRef]
16. Zhou, D.; Spee, R.; Alexander, G.C. Experimental evaluation of a rotor flux oriented control algorithm for brushless doubly-fed machines. *IEEE Trans. Power Electron.* **1997**, *12*, 72–78. [CrossRef]
17. Huang, S.D.; Huang, K.Y.; Lawu, Z.; Lieen, L. A study of the control strategy on rotor field orientation for brushless doubly-fed machine. In Proceedings of the IEEE Power Electron. Motion Control Conference, Beijing, China, 15–18 August 2000. [CrossRef]
18. Zhang, A.L.; Wang, X.; Jia, W.X.; Ma, Y. Indirect Stator-Quantities Control for the Brushless Doubly Fed Induction Machine. *IEEE Trans. Power Electron.* **2014**, *29*, 1392–1401. [CrossRef]
19. Chen, H.; Jiang, B.; Ding, S.X.; Huang, B. Data-driven fault diagnosis for traction systems in high-speed trains: A survey, challenges, and perspectives. *IEEE Trans. Intell. Transp. Syst.* **2022**, *23*, 1700–1716. [CrossRef]
20. Poza, J.; Oyarbide, E.; Roye, D. New vector control algorithm for brushless doubly-fed machines. In Proceedings of the IEEE 2002 28th Annual Conference of the Industrial Electronics Society, Seville, Spain, 5–8 November 2002. [CrossRef]
21. Zhang, G.G.; Yang, J.; Sun, Y.; Su, M.; Tang, W.Y.; Zhu, Q.; Wang, H. A Robust Control Scheme Based on ISMC for the Brushless Doubly Fed Induction Machine. *IEEE Trans. Power Electron.* **2018**, *33*, 3129–3140. [CrossRef]
22. Hopfensperger, B.; Atkinson, D.J.; Lakin, R.A. Stator flux-oriented control of a cascaded doubly fed induction machine. *IET Electr. Power Appl.* **1999**, *146*, 597–605. [CrossRef]
23. Sun, L.; Chen, Y.; Su, J.J.; Zhang, D.B.; Peng, L.; Kang, Y. Decoupling Network Design for Inner Current Loops of Stand-Alone Brushless Doubly Fed Induction Generation Power System. *IEEE Trans. Power Electron.* **2018**, *33*, 957–963. [CrossRef]
24. Wei, X.C.; Cheng, M.; Wang, W.; Han, P.; Luo, R.S. Direct Voltage Control of Dual-Stator Brushless Doubly Fed Induction Generator for Stand-Alone Wind Energy Conversion Systems. *IEEE Trans. Magn.* **2016**, *52*, 1–4. [CrossRef]
25. Xia, C.Y.; Guo, H.Y. Feedback linearization control approach for Brushless Doubly-Fed Machine. *Int. J. Precis. Eng. Manuf.* **2015**, *16*, 1699–1709. [CrossRef]
26. Xia, C.Y.; Zhang, Y.H.; Guo, H.Y. Brushless doubly-fed motor feedback linearization control method. *Trans. China Electro-Tech. Soc.* **2020**, *35*, 1387–1397. [CrossRef]
27. Xia, C.Y.; Hou, X.X. Study on the Static Load Capacity and Synthetic Vector Direct Torque Control of Brushless Doubly Fed Machines. *Energies* **2016**, *16*, 966. [CrossRef]
28. Li, Y.; Xu, S.Q.; Chen, H.T.; Jia, L.; Ma, K. A General Degradation Process of Useful Life Analysis Under Unreliable Signals for Accelerated Degradation Testing. *IEEE Trans. Ind. Inform.* **2022**, 1–9. [CrossRef]
29. Shi, J.N.; Xia, C.Y. Feedback Linearization and Maximum Torque per Ampere Control Methods of Cup Rotor Permanent-Magnet Doubly Fed Machine. *Energies* **2021**, *14*, 6402. [CrossRef]
30. Wang, N.N. Performance Analysis of Vector Control of Brushless Doubly-Fed Machine in Double Synchronous Reference Frame. In Proceedings of the 2022 25th International Conference on Electrical Machines and Systems (ICEMS), Chiang Mai, Thailand, 29 November–2 December 2022. [CrossRef]
31. Chen, H.T.; Chen, Z.W.; Chai, Z.; Jiang, B.; Huang, B. A single-side neural network-aided canonical correlation analysis with applications to fault diagnosis. *IEEE Trans. Cybern.* **2022**, *52*, 9454–9466. [CrossRef]